catalysts

MDPI

Article

Hierarchically Ordinated Two-Dimensional MoS_2 Nanosheets on Three-Dimensional Reduced Graphene Oxide Aerogels as Highly Active and Stable Catalysts for Hydrogen Evolution Reaction

Hyeonggeun Choi [1,†], Suok Lee [1,†], Min-Cheol Kim [2], Yeonsu Park [1], A-Rang Jang [3], Wook Ahn [1], Jung Inn Sohn [2], Jong Bae Park [4,*], John Hong [5,*] and Young-Woo Lee [1,*]

1 Department of Energy Systems Engineering, Soonchunhyang University, Asan-si 31538, Korea; rltk228@hanmail.net (H.C.); solee0117@gmail.com (S.L.); qkrdustn9807@naver.com (Y.P.); wahn21@sch.ac.kr (W.A.)
2 Division of Physics and Semiconductor Science, Dongguk University-Seoul, Seoul 04620, Korea; mcnet0618@dongguk.edu (M.-C.K.); junginn.sohn@dongguk.edu (J.I.S.)
3 Department of Electrical Engineering, Semyung University, Jecheon-si 27136, Korea; arjang@semyung.ac.kr
4 Jeonju Centre, Korea Basic Science Institute, Jeonju 54907, Korea
5 School of Materials Science and Engineering, Kookmin University, Seoul 02707, Korea
* Correspondence: jbpjb@kbsi.re.kr (J.B.P.); johnhong@kookmin.ac.kr (J.H.); ywlee@sch.ac.kr (Y.-W.L.); Tel.: +82-63-711-4517 (J.B.P.); +82-2-910-4665 (J.H.); +82-41-530-4988(Y.-W.L.)
† Those authors contributed equally to this work.

Citation: Choi, H.; Lee, S.; Kim, M.-C.; Park, Y.; Jang, A-R.; Ahn, W.; Sohn, J.-I.; Park, J.-B.; Hong, J.; Lee, Y.-W. Hierarchically Ordinated Two-Dimensional MoS_2 Nanosheets on Three-Dimensional Reduced Graphene Oxide Aerogels as Highly Active and Stable Catalysts for Hydrogen Evolution Reaction. *Catalysts* **2021**, *11*, 182. https://doi.org/10.3390/catal11020182

Academic Editor: Vincenzo Baglio
Received: 28 December 2020
Accepted: 28 January 2021
Published: 30 January 2021

Abstract: Hydrogen gas (H_2) is being intensively proposed as a next-generation clean energy owing to the depletion of fossil fuels. Electrochemical water splitting is one of the most promising processes for hydrogen production. Furthermore, many efforts focusing on electrochemical water splitting have been made to develop low-cost, electrochemically active, and stable catalysts for efficient hydrogen production. MoS_2 has emerged as an attractive material for developing catalysts for the hydrogen evolution reaction (HER). Hence, in this study, we design hierarchically ordinated two-dimensional (2D) MoS_2 nanosheets on three-dimensional (3D) reduced graphene oxide (rGO) (H-2D/3D-MoS_2-rGO) aerogel structures as a new class of electrocatalysts for the HER. We use the one-pot hydrothermal synthesis route for developing high-performance electroactive materials for the HER. The as-prepared H-2D/3D-MoS_2-rGO contains a unique 3D hierarchical structure providing large surface areas owing to the 3D porous networks of rGO and more active sites owing to the many edge sites in the MoS_2 nanosheets. In addition, the H-2D/3D-MoS_2-rGO structure exhibits remarkable electrochemical properties during the HER. It shows a lower overpotential than pure MoS_2 and excellent electrochemical stability owing to the large number of active sites (highly exposed edge sites) and high electrical conductivity from the rGO structure.

Keywords: molybdenum disulfide; reduced graphene oxide; 3D networks; electrocatalysts; hydrogen evolution reaction

1. Introduction

Hydrogen gas (H_2) is a promising renewable and inexhaustible energy source for replacing generally used fossil fuels [1–3]. In particular, the hydrogen evolution reaction (HER) process is crucial for hydrogen production. Platinum and other noble metal-based materials have proved to be the most attractive electrocatalysts for the HER, with high activity and durability in acidic or basic media [4–7]. However, in terms of the production cost of H_2 as per the price of Pt catalysts, the production of H_2 from noble Pt materials is not effective [8,9].

Therefore, in recent years, transition metal oxides/sulfides have emerged as effective alternatives to Pt and Pt-based electrocatalysts. Numerous studies have been devoted to

enhancing the electrochemical properties of transition metal oxides/sulfides/phosphides/carbides [10–28]. For example, Shen and Yin's research groups reported that the bimetallic nickel-cobalt phosphide shows improved HER activity and stability, due to its unique morphology with nanosheets on the 3D integrated framework, providing a large surface area and many active sites for HER [24]. In a recent works, among many HER catalyst candidates, two-dimensional MoS_2, an earth-abundant material, with its unique layered structure and chemical properties, has shown attractive HER catalytic activity with the corresponding electrolyte ion adsorption and desorption energies [10,11]. However, the basal plane of pure MoS_2 is catalytically inert, and only the edge S sites, occupying a small area in pure MoS_2, are catalytically active [29–34]. Therefore, increasing the number of active edges for forming large electrolyte ion adsorption/desorption sites and enhancing the electrical conductivity of pure MoS_2 for facile charge transport are the two main strategies for obtaining high HER catalytic activities.

Structural engineering of MoS_2 through the miniaturization of its size, shape, and dimensions is an effective and viable strategy for dramatically increasing the total number of edge sites, which are related to catalytic active sites. Mo-edge sites of MoS_2 can provide high electrochemical activity and exhibit the low free energy of hydrogen adsorption (ΔG_H^*) compared to inert adsorption sites at the basal plane of MoS_2 [10,31,35–37]. Therefore, many studies have focused on vertically grown MoS_2 sheets, MoS_2 nanostructures of different shapes, and various MoS_2 heterostructures for achieving a high density of edge sites [31,38–43]. Concurrently, controlling the conductivity of structurally engineered MoS_2 can synergistically improve its overall catalytic performance during the HER. In this regard, highly conductive materials such as carbon-based materials (e.g., graphene, carbon nanotubes) can be used as a subclass of conducting networks or substrates, because these materials can facilitate fast charge carrier transport, thus enhancing the HER activity [39,44–48]. In particular, reduced graphene oxide (rGO) is one of the most attractive materials for producing conducting templates because of its chemical stability, high conductivity, and excellent fabrication compatibility with solution-based processes [49–51]. Moreover, rGO can function as an excellent backbone network for constructing three-dimensionally dispersed catalytic materials [52–55]. However, it is challenging to develop the appropriate synthetic routes and fabrication steps for structural engineering of MoS_2 using conductive carbon materials, such as rGO, to achieve highly dispersed catalytic materials. These unique engineering approaches can be particularly beneficial in terms of enhancing the surface area, ion diffusion paths, and conductivity of the catalysts used for the HER.

Therefore, in this work, we developed a simple hydrothermal method to synthesize hierarchically ordinated two-dimensional (2D) MoS_2 nanosheets on three-dimensional (3D) rGO (H-2D/3D-MoS_2-rGO) aerogels. The proposed H-2D/3D-MoS_2-rGO heterostructures were fabricated via a one-pot and facile hydrothermal synthesis route. Moreover, through freeze-drying, the original 3D hydrogel structures were maintained without shrinkage deformation of H-2D/3D-MoS_2-rGO as it developed a unique light and hard aerogel structure during the drying process. The as-prepared H-2D/3D-MoS_2-rGO structures exhibited a large surface area and excellent HER catalytic activity because of the large number of active sites (highly exposed edge sites), highly dispersed MoS_2 nanosheets in the rGO networks, and high electrical conductivity, thus ensuring favorable electrochemical performance during the HER.

2. Results and Discussion

Figure 1 schematically illustrates the fabrication steps of the hierarchically ordinated H-2D/3D-MoS_2-rGO aerogels using the one-pot hydrothermal synthesis route. Figure 2a presents an illustration of the assembled H-2D/3D-MoS_2-rGO structures. The thin MoS_2 nanosheets are uniformly distributed on the backbone of the 3D rGO networks, which provide hierarchical structures. As mentioned in the introduction, a well-engineered MoS_2-based HER catalyst with a large surface area and high density of edge sites is

most important for achieving enhanced electrochemical activity in the HER. As shown in Figure 2a, the fabricated H-2D/3D-MoS_2-rGO electrode will show the superior electrochemical properties owing to its unique hierarchical structures consisting of the MoS_2 nanostructures and 3D porous rGO network, which can provide the enlarged surface area and active sites for HER, respectively. In addition, although the H-2D/3D-MoS_2-rGO has a highly porous network, the as-obtained H-2D/3D-MoS_2-rGO aerogel sustained an 8 mL glass vial (approximately 9 g) without any shape deformation (left side of Figure 2b). Moreover, the sample is very light (total weight of 239 mg and density of 45.1 mg cm^{-3}), enough so to be placed on a whole foxtail. These mechanical features are most important for the design and development of durable and light electrode materials from an economic perspective in the energy industry.

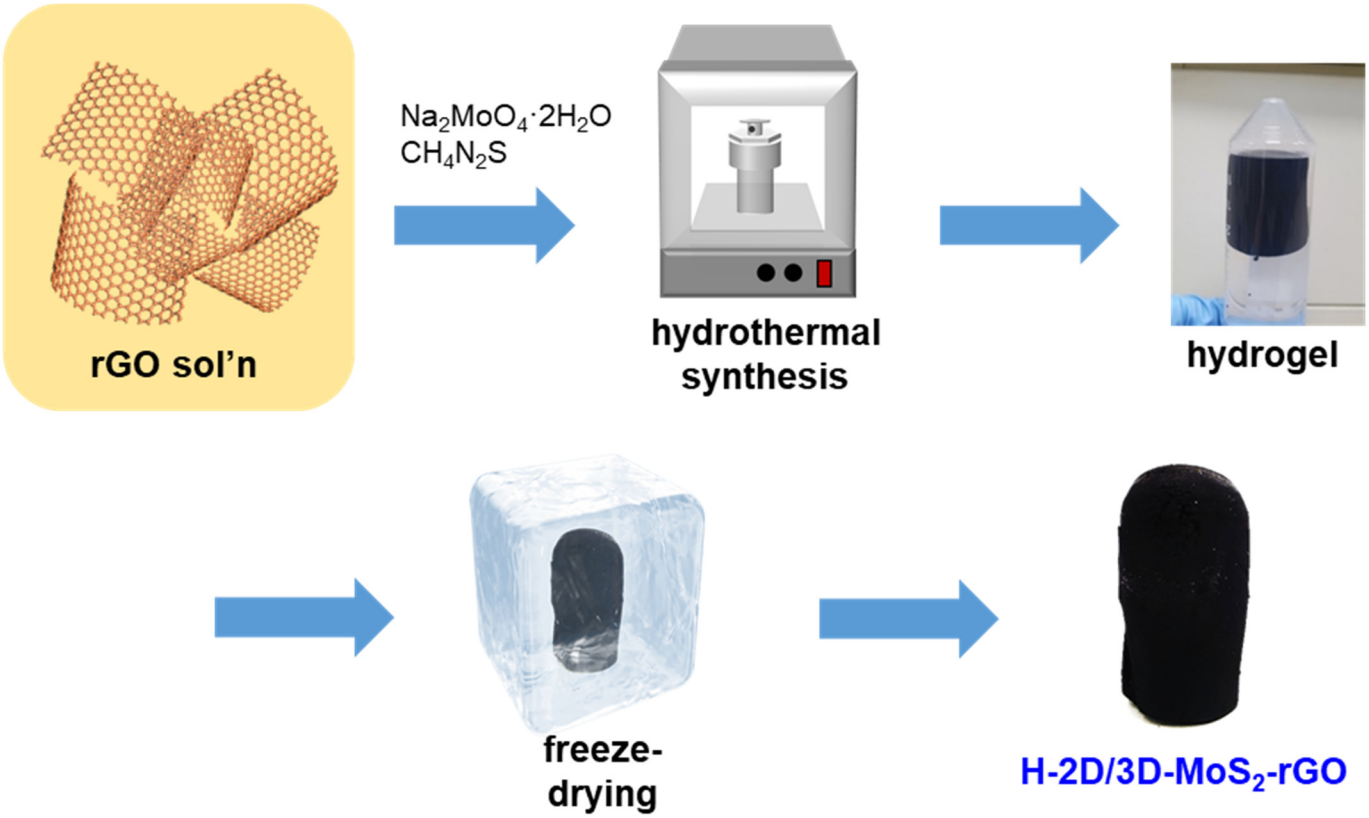

Figure 1. Schematic of the synthesis process for the H-2D/3D-MoS_2-rGO structures.

To confirm the 3D hierarchical structure of the H-2D/3D-MoS_2-rGO, we carried out SEM analysis. Figure 2c presents an SEM image of the as-obtained H-2D/3D-MoS_2-rGO samples. Extremely thin nanostructured rGO sheets with uniform and smooth surface morphology form an interconnected 3D microscale porous network. Moreover, small nanoscale MoS_2 sheets with sizes of 200–300 nm are uniformly distributed and deposited on the 3D porous networks of rGO. These unique interconnected 2D/3D structures might have resulted from the one-pot hydrothermal synthetic route and fast freeze-drying procedure, during which the H-2D/3D-MoS_2-rGO maintained its original aerogel structure without any deformation. Next, the elemental distributions of the H-2D/3D-MoS_2-rGO samples were identified via EDX elemental mapping analysis (Figure 2d). The Mo, S, and C elements are clearly observed throughout the sample, confirming that these elements are uniformly distributed among the hierarchical structures. The highly ordered structure and dispersion of MoS_2 might have provided a large surface area and many active edge sites to improve the overall electrochemical performance during the HER. Contrary to the H-2D/3D-MoS2-rGO, the pure MoS_2 synthesized without rGO appeared as micron-sized particles (Figure 3a), indicating that pure MoS_2 particles could have relatively low specific surface areas. In fact,

Brunauer–Emmett–Teller (BET) analysis (Figure 3b) revealed that the specific surface area of the H-2D/3D-MoS_2-rGO was 42.2 m^2 g^{-1}, which is approximately 2.7 times higher than that of pure MoS_2 (15.5 m^2 g^{-1}).

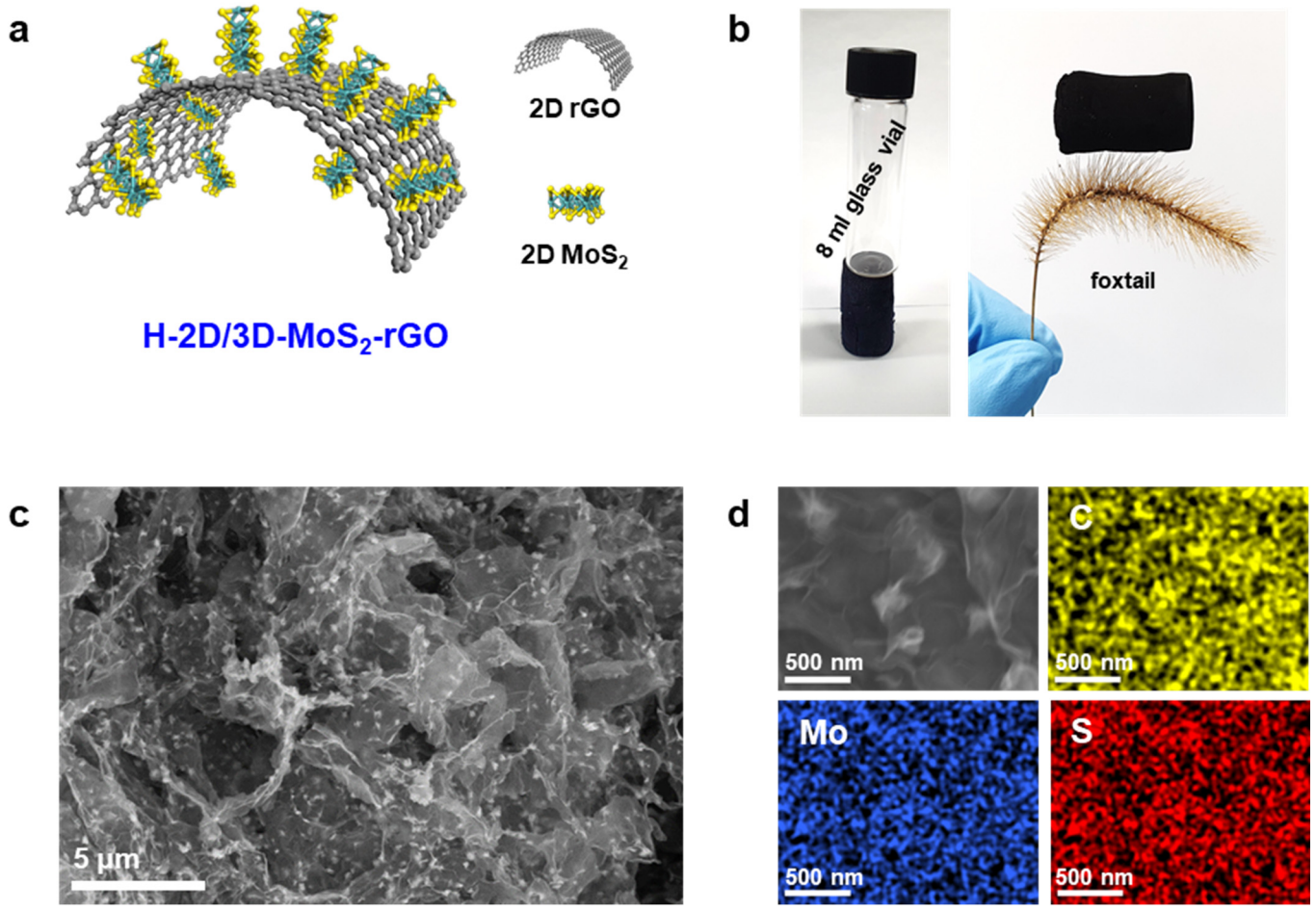

Figure 2. (**a**) Illustration of the 2D/2D assembled 3D porous network architectures. (**b**) Photographic image of H-2D/3D-MoS_2-rGO supporting the 8-mL glass vial and placed on the foxtail. (**c**) SEM image of H-2D/3D-MoS_2-rGO. (**d**) SEM and EDX elemental mapping images of H-2D/3D-MoS_2-rGO.

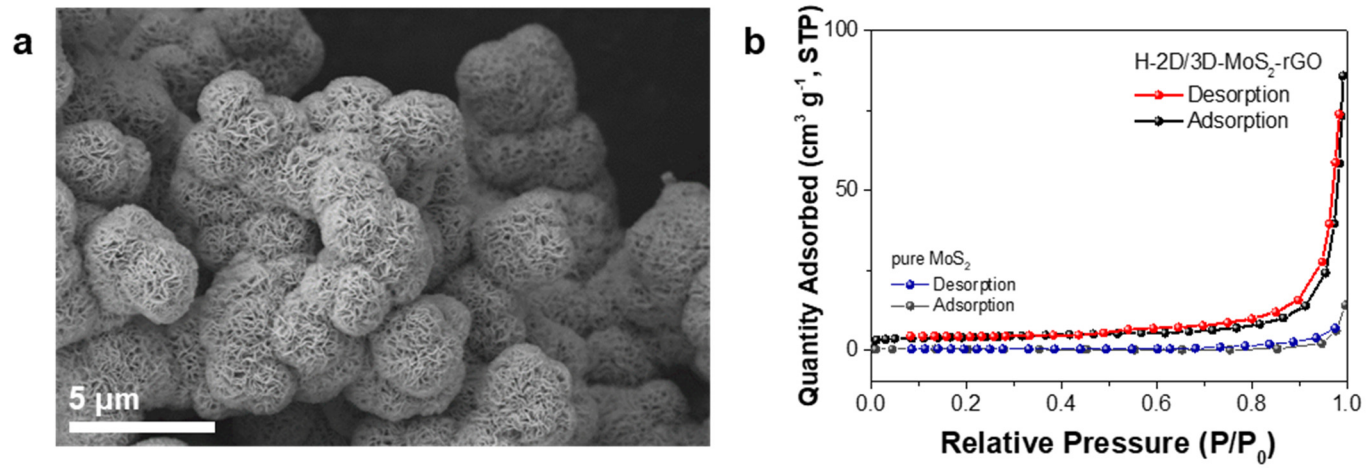

Figure 3. (**a**) SEM image of pure MoS_2. (**b**) Brunauer–Emmett–Teller (BET) curves for H-2D/3D-MoS_2-rGO and pure MoS_2.

To further verify the crystal and chemical structures of the H-2D/3D-MoS_2-rGO, XRD, Raman, and XPS analyses were also carried out. The XRD spectra of the H-2D/3D-MoS_2-rGO and pure MoS_2 are shown in Figure 4a. The reflection peaks for both samples can be assigned to the crystal lattice planes of hexagonal MoS_2 (JCPDS Card No. 77-1716) without any noticeable differences, confirming the high purity of the MoS_2 phase [30,56]. All the samples exhibit diffraction peaks at 2θ = 14.3°, 33.3°, 39.5°, 43.9°, and 58.5°, which can be clearly assigned to the (002), (100), (103), (104), and (110) planes of the MoS_2 phase, respectively. Figure 4b shows the Raman spectra of the as-prepared samples. For the H-2D/3D-MoS_2-rGO and pure rGO samples, two representative peaks can be identified at ~1348 and 1583 cm^{-1}, which correspond to the characteristic D and G bands, respectively [39,56]. For the H-2D/3D-MoS_2-rGO and pure MoS_2 samples, two peaks were clearly observed at ~379 and ~405 cm^{-1}, which are in accordance with the in-plane (E^1_{2g}) and out-of-plane (A_{1g}) modes, respectively [39,57]. It is highly expected that the H-2D/3D-MoS_2-rGO electrode will contribute to the improved electrochemical properties in HER due to its excellent structural features from the crystalline MoS_2 and rGO. To clearly reveal the presence of the corresponding elements, we carried out X-ray photoelectron spectroscopy (XPS) analysis. Figure 4c presents the high-resolution XPS spectra of the Mo 3d, S 2p, and C 1s regions with the fitted peak components. First, the Mo 3d doublet is clearly observed at ~229.4 eV (Mo^{4+} $2d_{5/2}$) and at ~232.6 eV (Mo^{4+} $2d_{3/2}$) [33,44,48,56,57]. Moreover, the two peaks at binding energies of ~163.5 and ~162.3 eV correspond to S^{2+} with the p spin-orbit splitting, indicating the existence of MoS_2 phase [33,44,48,57]. In addition, the XPS spectrum of C 1s for the H-2D/3D-MoS_2-rGO was deconvoluted into the four peaks located at around 284.5 eV (C–C), 285.6 eV (C–O), 287.0 eV (C=O), 288.6 eV (O=C–O), and 290.8 eV [44,48,56,58]. In particular, the intensive peak at around 284.5 eV corresponded to the C–C bond, revealing that the GO particles were converted to the rGO network. Thus, a comparison of the SEM, EDX, XRD, Raman, and XPS results provides direct evidence for the formation of the hierarchically ordinated H-2D/3D-MoS_2-rGO aerogels.

To evaluate their electrochemical performance, the H-2D/3D-MoS_2-rGO and pure MoS_2 samples were applied directly as working electrodes. Moreover, a Pt/C electrode was used as the reference electrode to objectively compare the performances of the as-synthesized H-2D/3D-MoS_2-rGO and pure MoS_2 electrodes. The corresponding HER polarization linear sweep voltammetry (LSV) curves and Tafel plots of both samples are shown in Figure 5a,b, respectively. Notably, the H-2D/3D-MoS_2-rGO sample exhibits a relatively low overpotential of 286 mV at a current density of 10 mA cm^{-2} compared to pure MoS_2. To further understand the improved catalytic behavior of the H-2D/3D-MoS_2-rGO structure, the Tafel plots and calculated Tafel slopes for the H-2D/3D-MoS_2-rGO and pure MoS_2 samples were derived from the polarization curves. As observed in Figure 5b, H-2D/3D-MoS_2-rGO delivers a Tafel slope of 77 mV dec^{-1}, which is obviously lower than that that of pure MoS_2 (125 mV dec^{-1}) and other MoS_2-based literatures (summarized in Table 1) [53,56–59]. The improved performance during the HER could be attributed to the increased number of active sites resulting from the hierarchically designed structure utilizing the 2D MoS_2 and 3D porous networks of rGO, where the ion adsorption and desorption processes could occur. Moreover, the high electrical conductivity of 3D rGO could have enhanced the overall electrochemical performance (Figure 5c). Finally, cycling tests of H-2D/3D-MoS_2-rGO were conducted to investigate its electrochemical stability during the HER. As shown in Figure 5d, the H-2D/3D-MoS_2-rGO electrode shows only a slight HER activity loss (~7 mV increase in the overpotential at a current density of 10 mA cm^{-2}) for 20 h. In addition, the initial performance of H-2D/3D-MoS_2-rGO was well maintained even after the 40 h electrochemical test (Figure 5e), confirming its high stability in acidic media for the HER.

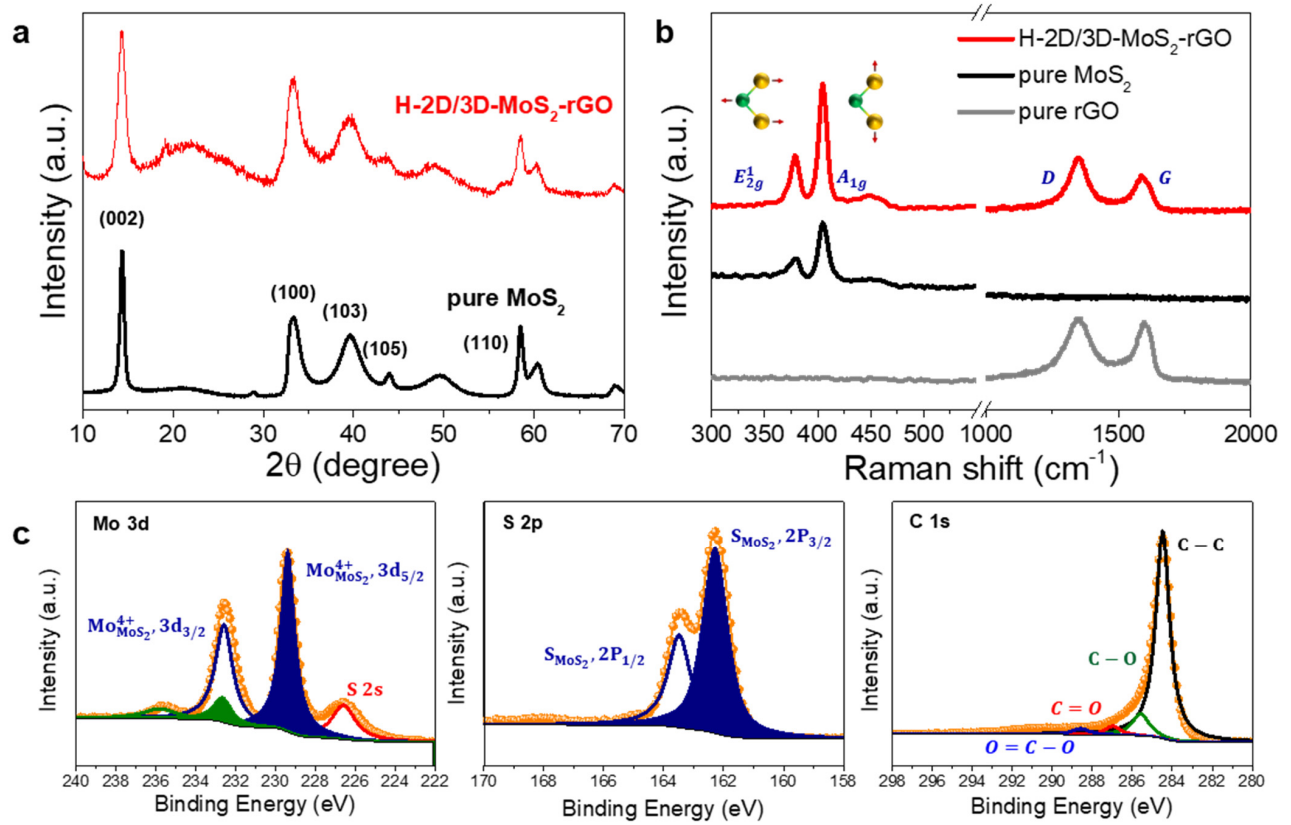

Figure 4. (**a**) XRD patterns for H-2D/3D-MoS_2-rGO and pure MoS_2. (**b**) Raman spectra for H-2D/3D-MoS_2-rGO, pure MoS_2, and pure rGO. (**c**) XPS spectra showing Mo 3d, S 2p, and C 1s in H-2D/3D-MoS_2-rGO.

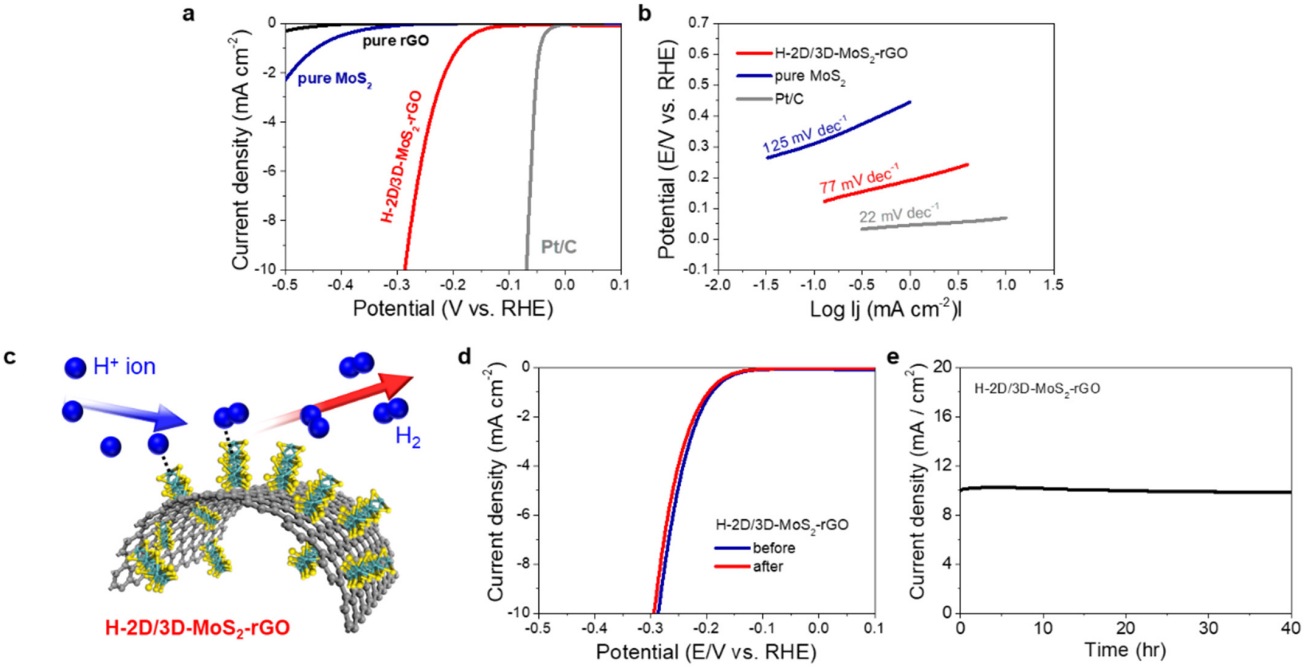

Figure 5. (**a**) Linear sweep voltammetry (LSV) curves for H-2D/3D-MoS_2-rGO, pure MoS_2, pure rGO, and Pt/C at a scan rate of 5 mVs^{-1} in 0.5 M H_2SO_4 electrolyte. (**b**) Tafel plots for H-2D/3D-MoS_2-rGO, pure MoS_2, and Pt/C. (**c**) Schematic illustration of the HER reaction process on H-2D/3D-MoS_2-rGO. (**d**) Comparison of LSV curves for the H-2D/3D-MoS_2-rGO before and after electrochemical stability tests. (**e**) Time dependence of current density for the H-2D/3D-MoS_2-rGO.

Table 1. Comparison of HER catalytic activities for the H-2D/3D-MoS_2-rGO and other reported MoS_2-based catalysts.

Materials	Overpotential (mV vs. RHE)	Tafel Slope (mV dec^{-1})	Reference
MoS_2Ag/rGO	290	102	[53]
3D MoS_2/N-GAs	261	230	[58]
hierarchical MoS_2–rGO nanosheets	250	98	[59]
3D MoS_2/rGO	>300	92	[56]
G@MoS_2	302	112	[57]
H-2D/3D-MoS_2-rGO	286	77	This work

3. Materials and Methods

3.1. Synthesis of H-2D/3D-MoS_2-rGO

To synthesize the H-2D/3D-MoS_2-rGO aerogels, commercially available GO was first modified from graphite powder (Graphene supermarket, Ronkonkoma, NY, USA) using the Hummers method to increase its surface area [60–62]. Three grams of graphite powder, 3 g of sodium nitrate ($NaNO_3$, Sigma-Aldrich, Saint Louis, MO, USA), and 100 mL of sulfuric acid (H_2SO_4, Sigma-Aldrich, Saint Louis, MO, USA) were mixed, and then 10 g potassium permanganate ($KMnO_4$, Sigma-Aldrich, Saint Louis, MO, USA) was slowly mixed in an ice bath. Next, the solution was continuously stirred to oxidize the graphite powder for 1 h at 95 °C. The resulting solution was diluted with distilled water, and 5 mL of hydrogen peroxide (30% H_2O_2, Sigma-Aldrich, Saint Louis, MO, USA) was added to the solution. Finally, to purify, the resulting solution was rinsed with 5% hydrochloric acid (HCl, Sigma-Aldrich, Saint Louis, MO, USA) and D.I water to obtain the graphite oxide (GO). The surface-treated GO was dispersed in distilled water at a concentration of 5 mg mL^{-1}. The H-2D/3D-MoS_2-rGO structures were prepared via one-pot hydrothermal synthesis. First, 309 mg sodium molybdate dihydrate ($Na_2MoO_4{\cdot}2H_2O$, Sigma-Aldrich, Saint Louis, MO, USA) and 971 mg thiourea (CH_4N_2S, Sigma-Aldrich, Saint Louis, MO, USA) were dissolved in deionized water and 17.5 mL of the GO solution. The mixture was transferred into a Teflon-lined stainless-steel autoclave (iNexus, Inc., Seongnam-si, Gyeonggi-do, Korea) and then kept at 200 °C for 12 h. After natural cooling, we obtained the H-2D/3D-MoS_2-rGO hydrogels. Finally, to form the H-2D/3D-MoS_2-rGO aerogels, the hydrogel was freeze-dried for 48 h using a freeze dryer (FDB-5503, OPERON, Gimpo-si, Gyeonggi-do, Republic of Korea).

3.2. Characterization and Electrochemical Measurements

The structural features and elemental distributions of the as-prepared samples were analyzed using field-emission scanning electron microscopy and energy-dispersive X-ray spectroscopy (FE-SEM and EDX, Gemini SEM 300, ZEISS). The Brunauer–Emmett–Teller (BET) surface areas of the synthesized samples were analyzed through nitrogen sorption measurements (Belsorp mini X, MicrotracBEL Corp.). The crystalline structures of the as-prepared samples were examined via powder X-ray diffraction (XRD Miniflex 600, RIGAKU) and Raman spectroscopy (AXIS NOVA, Kratos, Korea Basic Science Institute-Jeonju Center). The surface chemical states of the H-2D/3D-MoS_2-rGO were characterized by X-ray photoelectron spectroscopy (XPS, AXIS NOVA, Kratos, Korea Basic Science Institute-Jeonju center). Electrochemical analyses of the as-prepared samples were carried out using a potentiostat (PGSTAT302N, Metrohm, Autolab) in a three-electrode system with a graphite rod (Metrohm, Autolab) as the counter electrode and an Ag/AgCl electrode (in saturated 3 M KCl, Metrohm, Autolab) as the reference electrode in a 0.5 M H_2SO_4 electrolyte solution (Sigma-Aldrich, Saint Louis, MO, USA). The loading mass on the glass carbon working electrode for pure MoS_2, H-2D/3D-MoS_2-rGO, and Pt/C is 150 μg_{total} cm^{-2}, 150 μg_{total} cm^{-2}, and 20 μg_{Pt} cm^{-2}, respectively.

4. Conclusions

In summary, we successfully designed and developed hierarchically ordinated 2D MoS_2 nanosheets on 3D rGO aerogels via a one-pot hydrothermal synthesis route to achieve improved catalytic performance during the HER. Through various microscopic and spectroscopic investigations, we confirmed that the as-prepared H-2D/3D-MoS_2-rGO has a 3D hierarchical structure, which can provide large surface areas owing to the 3D porous networks of rGO and more active sites owing to the many edges of the MoS_2 nanosheets. Therefore, the developed H-2D/3D-MoS_2-rGO exhibited good electrochemical performance during the HER, showing a lower overpotential than pure MoS_2 and high electrochemical stability. Thus, it is expected that the as-prepared H-2D/3D-MoS_2-rGO structures can be used as highly active and stable electrode materials in acidic HER systems.

Author Contributions: Conceptualization and data curation, H.C., S.L. and Y.-W.L.; formal analysis, M.-C.K., Y.P. and A.-R.J.; investigation, W.A. and J.I.S.; writing—original draft preparation, J.H. and Y.-W.L.; writing—review and editing, J.B.P., J.H. and Y.-W.L. All authors have read and agreed to the published version of the manuscript.

Funding: This research was supported by a National Research Foundation of Korea grant funded by the Korean government (MSIT) (2019M1A2A2065616) and by the Soonchunhyang University Research Fund.

Conflicts of Interest: The authors declare no conflict of interest.

References

1. Turner, J.A. A realizable renewable energy future. *Science* **1999**, *285*, 687–689. [CrossRef] [PubMed]
2. Schlapbach, L. Hydrogen-fuelled vehicles. *Nature* **2009**, *406*, 809–811. [CrossRef] [PubMed]
3. Dutta, S. A review on production, storage of hydrogen and its utilization as an energy resource. *J. Ind. Eng. Chem.* **2014**, *20*, 1148–1156. [CrossRef]
4. Greeley, J.; Jaramillo, T.F.; Bonde, J.; Chorkendorff, I.; Nørskov, J.K. Computational high-throughput screening of electrocatalytic materials for hydrogen evolution. *Nat. Mater.* **2006**, *5*, 909–913. [CrossRef]
5. Nørskov, J.K.; Bligaard, T.; Logadottir, A.; Kitchin, J.R.; Chen, J.G.; Pandelov, S.; Stimming, U. Trends in the exchange current for hydrogen evolution. *J. Electrochem. Soc.* **2005**, *152*, 23–26. [CrossRef]
6. Lee, Y.W.; Ko, A.R.; Han, S.B.; Kim, H.S.; Park, K.W. Synthesis of octahedral Pt–Pd alloy nanoparticles for improved catalytic activity and stability in methanol electrooxidation. *Phys. Chem. Chem. Phys.* **2011**, *13*, 5569–5572. [CrossRef]
7. Lee, Y.W.; Ko, A.R.; Kim, D.Y.; Han, S.B.; Park, K.W. Octahedral Pt-Pd alloy catalysts with enhanced oxygen reduction activity and stability in proton exchange membrane fuel cells. *RSC Adv.* **2012**, *2*, 1119–1125. [CrossRef]
8. Jiang, Z.; Ren, J.; Li, Y.; Zhang, X.; Zhang, P.; Huang, J.; Du, C.; Chen, J. Low-cost high-performance hydrogen evolution electrocatalysts based on Pt-CoP polyhedra with low Pt loading in both alkaline and neutral media. *Dalton Trans.* **2019**, *48*, 8920–8930. [CrossRef]
9. Seh, Z.W.; Kibsgaard, J.; Dickens, C.F.; Chorkendorff, I.; Nøskov, J.K.; Seh, T.F. Combining theory and experiment in electrocatalysis: Insights into materials design. *Science* **2017**, *355*, eaad4998. [CrossRef]
10. Hinnemann, B.; Moses, P.G.; Bonde, J.; Jørgensen, K.P.; Nielsen, J.H.; Horch, S.; Chorkendorff, I.; Nørskov, J.K. Biomimetic hydrogen evolution: MoS_2 nanoparticles as catalyst for hydrogen evolution. *J. Am. Chem. Soc.* **2005**, *127*, 5308–5309. [CrossRef]
11. Jaramillo, T.F.; Jørgensen, K.P.; Bonde, J.; Nielsen, J.H.; Horch, S.; Chorkendorff, I. Identification of active edge sites for electrochemical H_2 evolution from MoS_2 nanocatalysts. *Science* **2017**, *317*, 100–102. [CrossRef] [PubMed]
12. Merki, D.; Hu, X.L. Recent developments of molybdenum and tungsten sulfides as hydrogen evolution catalysts. *Energy Environ. Sci.* **2011**, *4*, 3878–3888. [CrossRef]
13. Lee, S.; Kwak, D.H.; Han, S.B.; Hwang, E.T.; Kim, M.C.; Lee, J.Y.; Lee, Y.W.; Park, K.W. Synthesis of hollow carbon nanostructures as a non-precious catalyst for oxygen reduction reaction. *Electrochim. Acta* **2016**, *191*, 805–812. [CrossRef]
14. Laursen, A.B.; Kegnaes, S.; Dahl, S.; Chorkendorff, I. Molybdenum sulfides-efficient and viable materials for electro- and photoelectrocatalytic hydrogen evolution. *Energy Environ. Sci.* **2012**, *5*, 5577–5591. [CrossRef]
15. Kibsgaard, J.; Chen, Z.; Reinecke, B.N.; Jaramillo, T.F. Engineering the surface structure of MoS_2 to preferentially expose active edge sites for electrocatalysis. *Nat. Mater.* **2012**, *11*, 963–969. [CrossRef]
16. Vrubel, H.; Hu, X. Growth and activation of an amorphous molybdenum sulfide hydrogen evolving catalyst. *ACS Catal.* **2013**, *3*, 2002–2011. [CrossRef]
17. Park, K.W.; Lee, Y.W.; Oh, J.K.; Kim, D.Y.; Han, S.B.; Ko, A.R.; Kim, S.J.; Kim, H.S. TiO_2-based nanowire supported catalysts for methanol electrooxidation in direct methanol fuel cells. *J. Ind. Eng. Chem.* **2011**, *17*, 696–699. [CrossRef]

18. Xie, J.; Zhang, J.; Li, S.; Grote, F.; Zhang, X.; Zhang, H.; Wang, R.; Lei, Y.; Pan, B.; Xie, Y. Controllable disorder engineering in oxygen-incorporated MoS_2 ultrathin nanosheets for efficient hydrogen evolution. *J. Am. Chem. Soc.* **2013**, *135*, 17881–17888. [CrossRef]
19. Jo, S.H.; Lee, Y.W.; Hong, J.; Sohn, J.I. Simple and facile fabrication of anion-vacancy-induced MoO_{3-X} catalysts for enhanced hydrogen evolution activity. *Catalysts* **2020**, *10*, 1180. [CrossRef]
20. Voiry, D.; Yamaguchi, H.; Li, J.; Silva, R.; Alves, D.C.B.; Fujita, T.; Chen, M.; Asefa, T.; Shenoy, V.B.; Eda, G.; et al. Enhanced catalytic activity in strained chemically exfoliated WS_2 nanosheets for hydrogen evolution. *Nat. Mater.* **2013**, *12*, 850–855. [CrossRef]
21. Ko, A.R.; Kim, J.Y.; Oh, J.K.; Lee, Y.W.; Han, S.B.; Park, K.W. Synergy effect of nanostructure electrodes supported by tungsten carbide and oxide for methanol electrooxidation. *Phys. Chem. Chem. Phys.* **2010**, *12*, 15181–15183. [CrossRef] [PubMed]
22. Lukowski, M.A.; Daniel, A.S.; English, C.R.; Meng, F.; Forticaux, A.; Hamers, R.J.; Jin, S. Highly active hydrogen evolution catalysis from metallic WS_2 nanosheet. *Energy Environ. Sci.* **2014**, *7*, 2608–2613. [CrossRef]
23. Oh, J.K.; Lee, Y.W.; Han, S.B.; Ko, A.R.; Kim, D.Y.; Kim, H.S.; Kim, S.J.; Roh, B.W.; Hwang, I.C.; Park, K.W. 3-Dimensional TiO_2 nanostructure supports and their improved electrochemical properties in methanol electrooxidation. *Catal. Sci. Technol.* **2011**, *1*, 394–396. [CrossRef]
24. Yu, C.; Xu, F.; Luo, L.; Abbo, H.S.; Titinchi, S.J.J.; Shen, P.K.; Tsiakaras, P.; Yin, S. Bimetallic Ni–Co phosphide nanosheets self-supported on nickel foam as high-performance electrocatalyst for hydrogen evolution reaction. *Electrochim. Acta* **2019**, *317*, 191–198. [CrossRef]
25. Jing, S.; Zhang, L.; Luo, L.; Lu, J.; Yin, S.; Shen, P.K.; Tsiakaras, P. N-doped porous molybdenum carbide nanobelts as efficient catalysts for hydrogen evolution reaction. *Appl. Catal. B-Environ.* **2018**, *224*, 533–540. [CrossRef]
26. Jing, S.; Lu, J.; Yu, G.; Yin, S.; Luo, L.; Zhang, Z.; Ma, Y.; Chen, W.; Shen, P.K. Carbon-encapsulated WO_x hybrids as efficient catalysts for hydrogen evolution. *Adv. Mater.* **2018**, *30*, 1705979. [CrossRef]
27. Wang, D.; Lu, J.; Luo, L.; Jing, S.; Abbo, H.S.; Titinchi, S.J.J.; Chen, Z.; Tsiakaras, P.; Yin, S. Enhanced hydrogen evolution activity over microwave-assisted functionalized 3D structured graphene anchoring FeP nanoparticles. *Electrochim. Acta* **2019**, *317*, 242–249. [CrossRef]
28. Xu, F.; Lu, J.; Luo, L.; Yu, C.; Tang, Z.; Abbo, H.S.; Titinchi, S.J.J.; Zhu, J.; Shen, P.K.; Yin, S. Cu_2S-Cu_3P nanowire arrays self-supported on copper foam as boosting electrocatalysts for hydrogen evolution. *Energy Technol.* **2019**, *7*, 1800993. [CrossRef]
29. Benck, J.D.; Hellstern, T.R.; Kibsgaard, J.; Chakthranont, P.; Jaramillo, T.F. Catalyzing the hydrogen evolution reaction (HER) with molybdenum sulfide nanomaterials. *ACS Catal.* **2014**, *4*, 3957–3971. [CrossRef]
30. Chung, D.Y.; Park, S.K.; Chung, Y.H.; Yu, S.H.; Sung, Y.E. Edge-exposed MoS_2 nano-assembled structures as efficient electrocatalysts for hydrogen evolution reaction. *Nanoscale* **2014**, *6*, 2131–2136. [CrossRef]
31. Kong, D.S.; Wang, H.T.; Cha, J.J.; Pasta, M.; Koski, K.J.; Yao, J.; Cui, Y. Synthesis of MoS_2 and $MoSe_2$ films with vertically aligned layers. *Nano Lett.* **2013**, *13*, 1341–1347. [CrossRef] [PubMed]
32. Yan, K.; Lu, Z.; Prinz, F.B.; Hsu, P.C.; Bradshaw, D.; Kong, D.; Wang, H.; Cui, Y.; Cha, J.J.; Zheng, G.; et al. Electrochemical tuning of vertically aligned MoS_2 nanofilms and it's application in improving hydrogen evolution reaction. *Proc. Natl. Acad. Sci. USA* **2013**, *110*, 19701–19706.
33. Yang, Y.; Fei, H.L.; Ruan, G.D.; Xiang, C.S.; Tour, J.M. Edge-oriented MoS_2 nanoporous films as flexible electrodes for hydrogen evolution reactions and supercapacitor devices. *Adv. Mater.* **2014**, *26*, 8163–8168. [CrossRef] [PubMed]
34. Li, H.; Wu, H.Q.; Yuan, S.G.; Qian, H. Synthesis and characterization of vertically standing MoS_2 nanosheets. *Sci. Rep.* **2016**, *6*, 21171. [CrossRef] [PubMed]
35. Ji, Q.; Zhang, Y.; Shi, J.; Zhang, Y.; Liu, Z. Morphological engineering of CVD-grown transition metal dichalcogenides for efficient electrochemical hydrogen evolution. *Adv. Mater.* **2016**, *28*, 6207–6212.
36. Park, T.; Bae, C.; Lee, H.; Leem, M.; Kim, H.; Ahn, W.; Kim, J.; Lee, E.; Shin, H.; Kim, H. Non-equilibrium fractal growth of MoS_2 for electrocatalytic hydrogen evolution. *CrystalEngComm* **2019**, *21*, 478–486. [CrossRef]
37. Qiu, X.; Huang, Y.; Nie, Z.; Ma, B.; Tan, Y.; Wu, Z.; Zhang, N.; Xie, X. Support interactions dictated active edge sites over MoS_2–carbon composites for hydrogen evolution. *Nanoscale* **2020**, *12*, 1109–1117. [CrossRef]
38. Shi, J.; Ma, D.; Han, G.; Zhang, Y.; Ji, Q.; Gao, T.; Sun, J.; Song, X.; Li, C.; Zhang, Y.; et al. Controllable growth and transfer of monolayer MoS_2 on Au foils and its potential application in hydrogen evolution reaction. *ACS Nano* **2014**, *8*, 10196–10204. [CrossRef]
39. Zheng, X.; Xu, J.; Yan, K.; Wang, H.; Wang, Z.; Yang, S. Space-confined growth of MoS_2 nanosheets within graphite: The layered hybrid of MoS_2 and graphene as an active catalyst for hydrogen evolution reaction. *Chem. Mater.* **2014**, *26*, 2344–2353. [CrossRef]
40. Zhang, B.; Jiu, J.; Wang, J.; Ruan, Y.; Ji, X.; Xu, K.; Chen, C.; Wan, H.; Miao, L.; Jiang, J. Interface engineering: The $Ni(OH)_2/MoS_2$ heterostructure for highly efficient alkaline hydrogen evolution. *Nano Energy* **2017**, *37*, 74–80. [CrossRef]
41. Li, Y.; Majewski, M.B.; Islam, S.M.; Hao, S.; Murthy, A.A.; DiStefano, J.G.; Hanson, E.D.; Xu, Y.; Wolverton, C.; Kanatzidis, M.G.; et al. Morphological engineering of winged Au@MoS_2 heterostructures for electrocatalytic hydrogen evolution. *Nano Lett.* **2018**, *18*, 7104–7110. [CrossRef] [PubMed]
42. Yu, Q.; Luo, Y.; Mahmood, A.; Liu, B.; Cheng, H.M. Engineering two-dimensional materials and their heterostructures as high-performance electrocatalysts. *Electrochem. Energy Rev.* **2019**, *2*, 373–394. [CrossRef]

43. Hu, J.; Zhang, C.; Zhang, Y.; Yang, B.; Qi, Q.; Sun, M.; Zi, F.; Leung, M.K.H.; Huang, B. Interface modulation of MoS_2/metal oxide heterostructures for efficient hydrogen evolution electrocatalysis. *Small* **2020**, *16*, 2002212. [CrossRef] [PubMed]
44. Li, D.J.; Maiti, U.N.; Lim, J.; Choi, D.S.; Lee, W.J.; Oh, Y.; Lee, G.Y.; Kim, S.O. Molybdenum sulfide/N-doped CNT forest hybrid catalysts for high-performance hydrogen evolution reaction. *Nano Lett.* **2014**, *14*, 1228–1233. [CrossRef]
45. Youn, D.H.; Han, S.; Kim, J.Y.; Kim, J.Y.; Park, H.; Choi, S.H.; Lee, J.S. Highly active and stable hydrogen evolution electrocatalysts based on molybdenum compounds on carbon nanotube−graphene hybrid support. *ACS Nano* **2014**, *8*, 5164–5173. [CrossRef]
46. Salarizadeh, P.; Askari, M.B.; Seifi, M.; Rozati, S.M. MoS_2 coating on different carbonaceous materials: Comparison of electrochemical properties and hydrogen evolution reaction performance. *J. Electroanal. Chem.* **2019**, *847*, 113198. [CrossRef]
47. Liao, L.; Zhu, J.; Bian, X.; Zhu, L.; Scanlon, M.D.; Girault, H.H.; Liu, B. MoS_2 formed on mesoporous graphene as a highly active catalyst for eydrogen evolution. *Adv. Funct. Mater.* **2013**, *23*, 5326–5333. [CrossRef]
48. Huang, J.; Chen, M.; Li, X.; Zhang, X.; Lin, L.; Liu, W.; Liu, Y. A facile layer-by-layer fabrication of three dimensional MoS_2-rGO-CNTs with high performance for hydrogen evolution reaction. *Electrochim. Acta* **2019**, *300*, 235–241. [CrossRef]
49. Tarcan, R.; Todor-Boer, O.; Petrovai, I.; Leordean, C.; Astilean, S.; Botiz, I. Reduced graphene oxide today. *J. Mater. Chem. C* **2020**, *8*, 1198–1224. [CrossRef]
50. Ahmad, H.; Fan, M.; Hui, D. Graphene oxide incorporated functional materials: A review. *Compos. Pt. B-Eng.* **2018**, *145*, 270–280. [CrossRef]
51. Smith, A.T.; Lachance, A.M.; Zeng, S.; Liu, B.; Sun, L. Synthesis, properties, and applications of graphene oxide/reduced graphene oxide and their nanocomposites. *Nano Mater. Sci.* **2019**, *1*, 31–47. [CrossRef]
52. Li, Y.; Wang, H.; Xie, L.; Liang, Y.; Hong, G.; Dai, H. MoS_2 nanoparticles grown on graphene: An advanced catalyst for the hydrogen evolution reaction. *J. Am. Chem. Soc.* **2011**, *133*, 7296–7299. [CrossRef] [PubMed]
53. Ma, C.-B.; Qi, X.; Chen, B.; Bao, S.Y.; Yin, Z.; Wu, X.-J.; Luo, Z.; Wei, J.; Zhang, H.-L.; Zhang, H. MoS_2 nanoflower-decorated reduced graphene oxide paper for high-performance hydrogen evolution reaction. *Nanoscale* **2014**, *6*, 5624–5629. [CrossRef]
54. Kamila, S.; Mohanty, B.; Samantara, A.K.; Guha, P.; Ghosh, A.; Jena, B.; Satyam, P.V.; Mishira, B.K.; Jana, B.K. Highly active 2D layered MoS_2-rGO hybrids for energy conversion and storage applications. *Sci. Rep.* **2017**, *7*, 8378–8390. [CrossRef]
55. Lee, J.E.; Jung, J.M.; Ko, T.Y.; Kim, S.; Kim, S.I.; Nah, J.; Ryu, S.; Nam, K.T.; Lee, M.H. Catalytic synergy effect of MoS_2/reduced graphene oxide hybrids for a highly efficient hydrogen evolution reaction. *RSC Adv.* **2017**, *7*, 5480–5487. [CrossRef]
56. Tang, C.; Zhong, L.; Zhang, B.; Wang, H.F.; Zhang, Q. 3D Mesoporous van der Waals Heterostructures for Trifunctional Energy Electrocatalysis. *Adv. Mater.* **2018**, *30*, 1705110. [CrossRef] [PubMed]
57. Liu, Y.; Zhu, Y.; Fan, X.; Wang, S.; Li, Y.; Zhang, F.; Zhang, G.; Peng, W. (0D3D) MoS_2 on porous graphene as catalysts for enhanced electrochemical hydrogen evolution. *Carbon* **2017**, *121*, 163–169. [CrossRef]
58. Hou, Y.; Zhang, B.; Wen, Z.; Cui, S.; Guo, X.; He, Z.; Chen, J. A 3D hybrid of layered MoS_2/nitrogen-doped graphene nanosheet aerogels: An effective catalyst for hydrogen evolution in microbial electrolysis cells. *J. Mater. Chem. A* **2014**, *2*, 13795. [CrossRef]
59. Zhou, J.; Xiao, H.; Zhou, B.; Huang, F.; Zhou, S.; Xiao, W.; Wang, D. Hierarchical MoS_2–rGO nanosheets with high MoS_2 loading with enhanced electro-catalytic performance. *Appl. Surf. Sci.* **2015**, *358*, 152–158. [CrossRef]
60. Lee, K.H.; Lee, Y.-W.; Lee, S.W.; Ha, J.S.; Lee, S.-S.; Son, J.G. Ice-templated self-assembly of $VOPO_4$-graphene nanocomposites for vertically porous 3D supercapacitor electrodes. *Sci. Rep.* **2015**, *5*, 13696. [CrossRef]
61. Hummers, W.S.; Offeman, R.E. Preparation of graphite oxide. *J. Am. Chem. Soc.* **1958**, *80*, 1339. [CrossRef]
62. Yu, H.; Zhang, B.; Bulin, C.; Li, R.; Xing, R. High-efficient synthesis of graphene oxide based on improved Hummers method. *Sci. Rep.* **2016**, *6*, 36143. [CrossRef] [PubMed]